Three-Dimensional Sparse Random Mode Decomposition for Mode Disentangling with Crossover Instantaneous Frequencies

Chen Luo[1], Tao Chen[1], Hongye Su[1], Luca Mainardi[2], Lei Xie[1]
[1]*State Key Laboratory of Industrial Control Technology, Zhejiang University, Hangzhou, China*
[2] *Department of Electronics, Information and Bioengineering, Politecnico di Milano, Milan, Italy*
Corresponding author: chentao227722@163.com, lxie@zju.edu.cn

***Abstract*—Sparse random mode decomposition (SRMD) is a novel algorithm that constructs a random time-frequency feature space to sparsely approximate spectrograms, effectively separating modes. However, it fails to distinguish adjacent or overlapped frequency components, especially, those with crossover instantaneous frequencies. To address this limitation, an enhanced version, termed three-dimensional SRMD (3D-SRMD), is proposed in this paper. In 3D-SRMD, the random features are lifted from a two-dimensional space to a three-dimensional (3D) space by introducing one extra chirp rate axis. This enhancement effectively disentangles the frequency components overlapped in the low dimension. Additionally, a novel random feature generation strategy is designed to improve the separation accuracy of 3D-SRMD by combining the 3D ridge detection method. Finally, numerical experiments on both simulated and real-world signals demonstrate the effectiveness of our method.**

***Index Terms*—sparse random mode decomposition, signal decomposition, chirp rate, crossover instantaneous frequency.**

I. Introduction

Non-stationary signals are ubiquitous in both natural [1], [2] and engineering systems [3], [4]. These signals are typically modeled as superpositions of amplitude and frequency-modulated modes, called multi-component signals (MCSs) [5]. To reveal the time-varying characteristics of these signals, time-frequency analysis (TFA) methods are introduced. A significant challenge within the TFA area is to separate the intrinsic modes within MCSs, commonly referred to as signal decomposition.

Initially, most decomposition methods directly extract intrinsic mode from MCSs in the time domain, e.g., the empirical mode decomposition [6] and its variants [7], [8]. However, these time-domain methods always lack mathematical foundations. On the other hand, since many real-world signals exhibit sparsity in the Fourier spectrum, variational mode decomposition [9] and its improved versions [10], [11] have been proposed to separate the intrinsic modes from MCSs in the frequency domain. However, these methods formulated in the frequency domain are unable to extract the wide-band modes that have an overlapping spectrum. Recently, to analyze wide-band signals, Chen et al. developed two advanced methods based on the multi-component chirp signal model, i.e., nonlinear chirp mode decomposition (NCMD) [12] and intrinsic chirp component decomposition (ICCD) [13].

More recently, sparse random mode decomposition (SRMD) was proposed as a novel signal decomposition method [14]. Inspired by the sparse random feature expansion [15], [16], SRMD begins by assuming that a signal can be approximately represented as the sum of sparse random time–frequency (TF) features. A spatial clustering algorithm is then utilized to separate the localized random features, thereby effectively achieving mode separation with less mode mixing and fewer Gibbs phenomena. However, adjacent or overlapped frequency components cannot be separated in the two-dimensional (2D) random feature space. Thus, SRMD is unable to disentangle modes with crossover instantaneous frequencies (IFs).

To address this issue, an improved method called three-dimensional SRMD (3D-SRMD) is proposed. Motivated by the chirplet transform (CT) [17]–[19], we lift the random features from the TF plane to a three-dimensional (3D) space, i.e., time-frequency-chirprate (TFC). This enhancement effectively disentangles the frequency components overlapped in the low dimension. Additionally, unlike SRMD, the concentrated generation of random features ensures the sparsity of the 3D random feature space and eliminates the dependence on clustering algorithms. By combining the 3D ridge detection (RD) method, this new random feature generation strategy effectively improves the mode separation of 3D-SRMD.

The remaining structure of this paper is outlined as follows: Section II recalls the fundamental theory of SRMD. The specific details of the proposed 3D-SRMD are delineated in Section III. Section IV presents numerical results both on simulated and real-world signals to demonstrate the superior performance of the proposed method.

II. Sparse Random Mode Decomposition

The SRMD is achieved on the sparse random feature approximation to the inverse short-time Fourier transform

This work was supported in part by the National Key R&D Program of China (No. 2022YFB3305900), the National Natural Science Foundation of P.R. China (NSFC: 62073286) and the Major Project of Science and Technology of Yunnan Province, China under Grant (202402AD080001)(*Chen Luo and Tao Chen contributed equally to this work.*) (*Corresponding author: Tao Chen; Lei Xie.*)

(STFT). Specifically, a signal $x(t) \in L^2(\mathbb{R})$ can be represented by:

$$x(t) = \int_{-\infty}^{+\infty} \int_{-\infty}^{+\infty} F_x^g(\tau, \xi) g(t-\tau) e^{j2\pi\xi t} d\tau d\xi, \quad (1)$$

where $F_x^g(\tau, \xi)$ denotes the STFT of $x(t)$ with $g(t)$; $g(t) \in L^2(\mathbb{R})$ is a (positive) window function such that $\int_{-\infty}^{+\infty} g(\tau) d\tau = 1$.

Employing the sparse random feature expansion, the signal can be approximated by random features (or basis) [15]:

$$\begin{aligned} x(t) &= \int_{-\infty}^{+\infty} \int_{-\infty}^{+\infty} F_x^g(\tau, \xi) g(t-\tau) e^{j2\pi\xi t} d\tau d\xi, \\ &\approx \sum_{i=1}^{N} c_i g(t-\tau_i) e^{j2\pi\xi_i t} = \sum_{i=1}^{N} c_i \varphi_i(t), \end{aligned} \quad (2)$$

where $(\tau_1, \xi_1), \cdots, (\tau_N, \xi_N)$ are drawn independently and identically distributed (i.i.d.) from a distribution $\mathcal{P}$ (chosen to be uniform in SRMD) with probability density function $p(\tau, \xi)$; $\varphi_i(t)$ represents the random feature; $c_i \in \mathbb{C}$ denotes the weight coefficients of $\varphi_i(t)$.

Reference [20] proved that, for any $\delta > 0$, with probability at least $1-\delta$ over $(\tau_1, \xi_1), \cdots, (\tau_N, \xi_N)$, there exist c_i such that the following approximation error bound in (2) holds:

$$\|x(t) - \sum_{i=1}^{N} c_i \varphi_i(t)\|_2 \leq \frac{C}{\sqrt{N}} (1 + \sqrt{2 \log \frac{1}{\delta}}), \quad (3)$$

where $C = \sup \frac{|F_x^g(\tau,\xi)|}{p(\tau,\xi)}$. This theory ensures the existence of c_i, paving the way for learning of optimal c_i through the construction of basis pursuit de-noising (BPDN) problem [21], [22] and its solution via the L1 norm spectral projection gradient (SPGL1) algorithm [23], [24].

In SRMD, (τ_i, ξ_i) with non-zero c_i obtained by the BPDN is expected to form a sparse TF representation of $x(t)$. These pairs with non-zero coefficients are then clustered using the density-based spatial clustering of applications with noise (DBSCAN) algorithm [25], thereby enabling the reconstruction of each mode based on the grouping of clusters, as follows:

$$x_k(t) = \sum_{i \in I_k} c_i^* \varphi_i(t), k = 1, \cdots, K, \quad (4)$$

where c_i^* is the coefficient obtained by solving the BPDN problem; K is the number of groups in the clustering results; I_k represents the index set of the k-th group of random features with non-zero coefficients.

III. Proposed Method

A. Three-Dimensional Random Feature Space

In (2), a specific pair of TF parameters (τ_i, ξ_i) uniquely determines a feature $\varphi_i(t)$. When the signal contains overlapped frequency components, the random features of different modes in the overlapped region have the same TF parameters. Consequently, it is impossible to separate the modes with crossover IFs in the 2D random TF feature space. Inspired by CT [17]–[19], we introduce chirp rate (CR) parameter to lift the random feature to TFC space. CR represents the rate at which frequency changes over time. When modes exhibit frequency crossover, they typically have distinct CRs at the crossover moment. Therefore, signals with overlapping frequency components, which entangle in 2D TF plane, can be separated in 3D TFC space (see Fig. 1 for an illustration).

Incorporating the CR into $\varphi_i(t)$ of (2), we obtain the 3D random features, as follows:

$$\breve{\varphi}_i(t) = g(t-\tau_i) e^{j2\pi\xi_i t} e^{j\pi\beta_i (t-\tau_i)^2}, \quad (5)$$

where β_i represents the newly introduced random chirp rate parameter. Similar to $\varphi_i(t)$, the random feature $\breve{\varphi}_i(t)$ corresponds to a specific tuple of TFC parameters (τ_i, ξ_i, β_i). Subsequently, a multitude of $\breve{\varphi}_i(t)$ constructs a 3D random feature space. Due to differences in TFC parameters, overlapped frequency components can be distinguished within this 3D space, ensuring the feasibility of separating modes with crossover IFs.

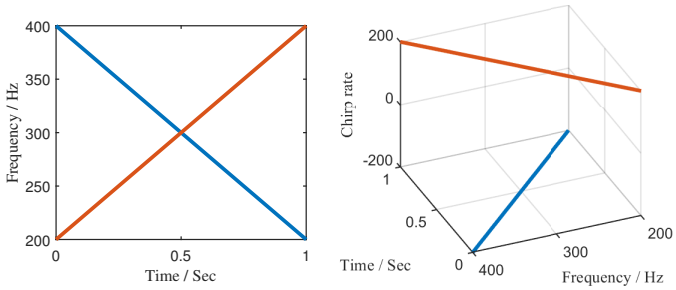

Fig. 1. The specific crossover frequency components $s_1 = \cos(2\pi(400t - 100t^2))$ and $s_2 = \cos(2\pi(200t + 100t^2))$ in (**left**) TF plane, (**right**) TFC space.

B. Concentrated Distribution of Random Features

Despite the enhancement in dimension should work theoretically, mode separation still fails due to the poor sparsity in the 3D random feature space (see Fig. 2 (**left**)) for an illustration). Therefore, we propose a concentrated distribution strategy to solve this issue.

Firstly, we consider a non-stationary MCS $x(t)$, defined as a superposition of AM-FM modes, as follows [12]:

$$\begin{aligned} x(t) &= \sum_{k=1}^{K} x_k(t) + e(t) \\ &= \sum_{k=1}^{K} a_k(t) \cos(2\pi \int_0^t f_k(\tau) d\tau + \phi_k) + e(t), \end{aligned} \quad (6)$$

where $t \in [0, L]$, L denotes the temporal duration of the signal; $K \in \mathbb{N}$ represents the number of intrinsic modes; $a_k(t) > 0$ and $f_k(t) > 0$ denote the instantaneous amplitude (IA) and IF of k-th mode; ϕ_k stands for the initial phase; $e(t)$ denotes the additive noise.

According to (2), the k-th mode in (6) can be approximated by the 2D random feature model as:

$$x_k(t) \approx \sum_{i=1}^{N} c_i^k g(t-\tau_i^k) e^{j2\pi\xi_i^k t}, \tag{7}$$

where the TF parameter pairs $(\tau_1^k, \xi_1^k), \cdots, (\tau_N^k, \xi_N^k)$ are drawn i.i.d. from a distribution $\mathcal{P}_k$ with $p_k(\tau, \xi)$; $\{c_1^k, \cdots, c_N^k\}$ denote the weight coefficient of model, which should be identified.

From (3), the approximation accuracy of the model is influenced by the error constant C, which decreases as $\mathcal{P}_k$ approximates the distribution associated with $\mid F_{x_k}^g(\tau, \xi) \mid$. Given that the STFT of $x_k(t)$ presents concentrated energy around its IF [26], $x_k(t)$ can be approximated with high accuracy by the model, whose random TF features are distributed around the IFs.

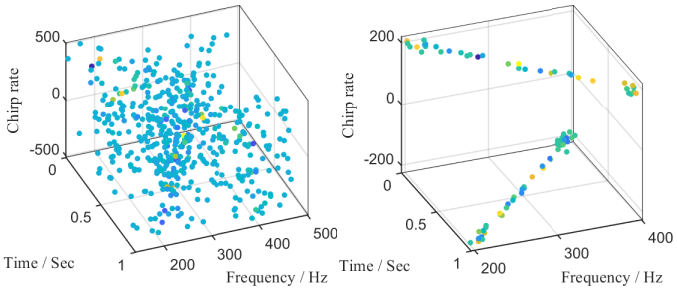

Fig. 2. The 3D random feature space of the signal in Fig. 1 with (**left**) uniform distribution and (**right**) concentrated distribution (color intensity indicates weight magnitude).

Similarly, assuming that $x_k(t)$ can be approximated by the 3D random feature model from (5), we have:

$$x_k(t) \approx \sum_{i=1}^{N} c_i^k g(t-\tau_i^k) e^{j2\pi\xi_i^k t} e^{j\pi\beta_i^k (t-\tau_i)^2}, \tag{8}$$

where $(\tau_1^k, \xi_1^k, \beta_1^k), \cdots, (\tau_N^k, \xi_N^k, \beta_N^k)$ are drawn i.i.d. from a distribution $\mathcal{Q}_k$ with $q_k(\tau, \xi, \beta)$. Like the 2D case, to achieve low approximation error, $\mathcal{Q}_k$ should be concentrated around the IF and CR of k-th mode. In this paper, $\mathcal{Q}_k$ is be considered as a band-limited uniform distribution, as follows:

$$q_k(\tau,\xi,\beta) = \begin{cases} \frac{1}{\lambda^2 L}, & \text{if } \tau \in [0, L], \\ & \xi \in [\widehat{f}_k(\tau) - \frac{\lambda}{2}, \widehat{f}_k(\tau) + \frac{\lambda}{2}], \\ & \beta \in [\widehat{f}_k'(\tau) - \frac{\lambda}{2}, \widehat{f}_k'(\tau) + \frac{\lambda}{2}], \\ 0, & \text{else}, \end{cases} \tag{9}$$

where $\widehat{f}_k(\tau)$ and $\widehat{f}_k'(\tau)$ represent the estimated IF and CR, λ represents the bandwidth parameter of q_k. Note that in this paper, 3D RD algorithm in [27] is applied to estimate IF and CR with the TFC representation generated by CT.

Random features for modes $x_1(t), \cdots, x_k(t)$ is generated by following $\mathcal{Q}_1, \cdots, \mathcal{Q}_k$, respectively, thereby ensuring the sparsity of the 3D random feature space (see Fig. 2 (**right**) for an illustration)). Furthermore, the random features corresponding to different modes are already separated by solving BPDN, thereby obviating the need for a clustering algorithm. Similar to (4), the mode can be reconstructed as follows:

$$x_k(t) = \sum_{i=1}^{N} c_i^{k^*} \breve{\varphi}_i^k(t), k = 1, \cdots, K, \tag{10}$$

where $c_i^{k^*}$ and $\breve{\varphi}_i^k(t)$ represent the coefficients and random features, which correspond to the k-th mode.

Algorithm 1 3D-SRMD

Input: Signal $\boldsymbol{x} = [x_1, \cdots, x_m]^T$, sampled time $\boldsymbol{t} = [t_1, \cdots, t_m]^T$, number of random features N, number of modes K ,window parameters α, bandwidth parameter λ.

1: Estimate the IFs $\widehat{f}_1(\tau), ..., \widehat{f}_K(\tau)$ and CRs $\widehat{f}_1'(\tau), ..., \widehat{f}_K'(\tau)$ by 3D RD algorithm.
2: Generate probability density function $q_1, ..., q_K$ as (9).
3: **for** $k = 1$ to K **do**
4: $\quad \{(\tau_i^k, \xi_i^k, \beta_i^k)\}_{i=1}^N$ are drawn i.i.d. from $\mathcal{Q}_k$ with q_k,
5: $\quad \{\phi_i^k\}_{i=1}^N \sim \mathcal{B}(1, 0.5)$.
6: **end for**
7: Construct the random feature matrix: $\Psi = [[\breve{\varphi}_i^1(\boldsymbol{t})] \cdots [\breve{\varphi}_i^K(\boldsymbol{t})]] \in \mathbb{R}^{m \times KN}$, $\breve{\varphi}_i^k(t)$ in (11).
8: Estimate the noise variance σ^2 of $\boldsymbol{x}$ by TF segmentation.
9: Solve the BPDN problem by SPGL1:
$\boldsymbol{c}^* = \underset{\boldsymbol{c}=[c_1^1 \cdots c_N^1 \cdots c_1^K \cdots c_N^K]^T \in \mathbb{R}^{KN}}{\arg\min} \|\boldsymbol{c}\|_1$
s.t. $\|\Psi \boldsymbol{c} - \boldsymbol{x}\|_2 \leq \sqrt{m}\sigma$.

Output: K modes $x_k(t) = \sum_{i=1}^{N} c_i^{k^*} \breve{\varphi}_i^k(t)$, $k = 1, \cdots, K$.

C. Algorithm Details

To reduce time consumption, we provide the real field version of the random features, as follows:

$$\breve{\varphi}_i^k(t) = g(t-\tau_i^k) \cos(2\pi\xi_i^k t + \pi\beta_i^k (t-\tau_i^k)^2 - \frac{\pi}{2}\phi_i^k), \tag{11}$$

where $\phi_i^k \sim \mathcal{B}(1, 0.5)$ serves as a unified replacement for the cosine and sine phases, capturing the real and imaginary components of the complex random features. Here, $g(t) = e^{-\frac{t^2}{2\alpha}}$ is chosen as a Gaussian window. It should be noted that, in practical applications, BPDN requires an estimation of the noise level in advance. Here, we adopt the TF segmentation algorithm of the rectified STFT in [28] as a noise estimator.

Finally, the complete 3D-SRMD algorithm is outlined in Algorithm 1.

D. Computational Complexity

As discussed above, the core of 3D-SRMD lies in solving the BPDN problem. In each iteration of the SPGL1 algorithm used for this purpose, the primary cost is divided into two parts [23]. First, the matrix-vector multiplications involving the dense random feature matrix Ψ and Ψ^T incur a cost of $O(mKN)$. Second, projecting the current point onto the ℓ_1-norm constraint ball, which employs a fast sorting heap structure, has a worst-case cost of $O(m \log m)$. Consequently, the total cost of 3D-SRMD is $O(mI(\log m + KN))$, where I denotes the total number of SPGL1 iterations.

IV. Numerical Results

In this section, both simulated and real-world signals with crossover modes are considered to compare the performance of 3D-SRMD with other methods, i.e., NCMD and ICCD.

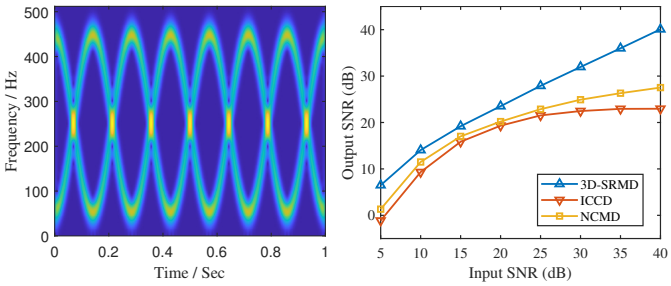

Fig. 3. (**left**) The TF spectrogram of the simulated signal by STFT; (**right**) output SNR vs. input SNR for different methods

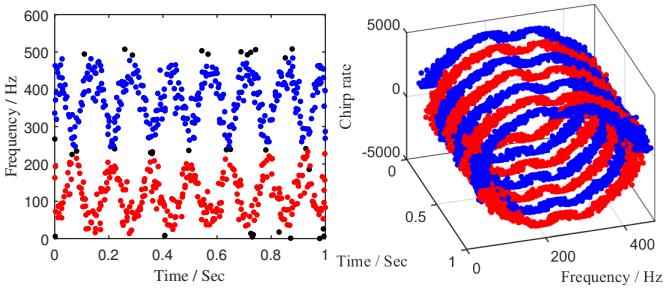

Fig. 4. The random feature space of the simulated signal in (**left**) SRMD and (**right**) 3D-SRMD (different colors signify different modes).

A. Simulated Signal

Firstly, we consider the synthetic signal, as follows:

$$s(t) = m_1(t) + m_2(t), \tag{12}$$

with

$$m_1(t) = \cos(2\pi(250t - \frac{200}{7\pi}\sin(7\pi t))), \tag{13}$$

$$m_2(t) = \cos(2\pi(250t + \frac{200}{7\pi}\sin(7\pi t))), \tag{14}$$

where the sampling frequency $f_s = 1024$ Hz and the time duration is $[0, 1]$ s. The IFs of two modes exhibit oscillatory patterns and intersect at multiple time points (see Fig. 3 (**left**)).

The parameters for each decomposition algorithm involved in the comparison are set as follows. Both NCMD and ICCD utilize the widely used IF estimation method RPRG [29], which is capable of estimating crossover IFs in the 2D TF plane. To ensure fairness, NCMD employs the same noise estimation as 3D-SRMD. In 3D-SRMD, we set $\alpha = L/80$, $N = 5000$, $\lambda = f_s/100$, and the maximum iteration count for the SPGL1 algorithm is set to 1000. In ICCD, a wider filter bandwidth should be chosen to improve the estimation accuracy of nonlinear oscillatory modes. Thus, we set $BW = f_s/10$, and the noise parameter is set to the default value of 5. Similarly, in NCMD, it is necessary to choose a larger penalty parameter to obtain a wider filter bandwidth, here set to $1\mathrm{e}{-2}$.

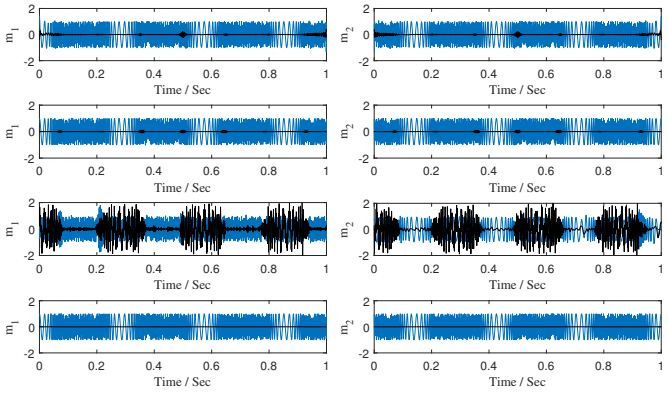

Fig. 5. Analysis results (blue: estimated modes; black: estimation errors) for the simulated signal by (**first row**) ICCD, (**second row**) NCMD, (**third row**) SRMD, (**last row**) 3D-SRMD. Note that the average SNR of the two signals by each method is 24.39 dB, 30.89 dB, 0.54 dB, and 55.70 dB, respectively.

Firstly, we evaluated the performance of each algorithm in a noise-free case. The decomposition results are shown in Fig. 4 and Fig. 5. Due to the influence of oscillating IFs, ICCD experiences errors at crossover points and edges. NCMD exhibits some errors at the crossover point caused by the estimated errors in IFs. SRMD reconstructs entirely erroneous modes, demonstrating its ineffectiveness in handling crossover IFs. Finally, the introduction of CR parameter enables 3D-SRMD to successfully decompose crossover modes, presenting the best decomposition performance among these methods.

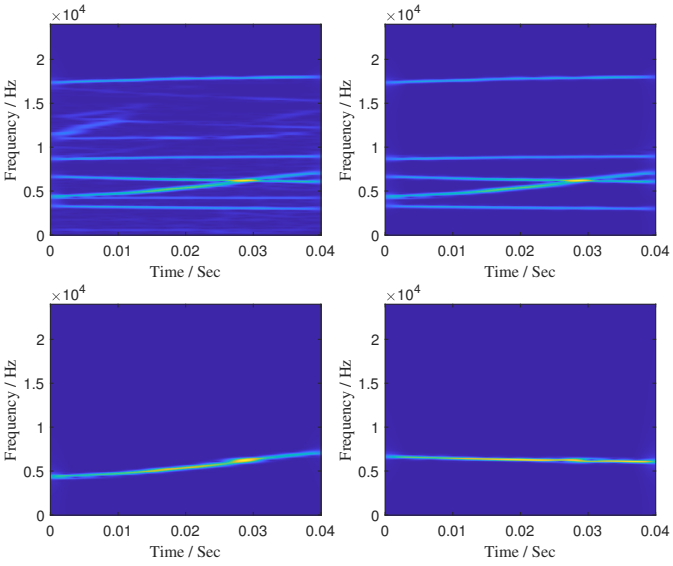

Fig. 6. The whales' whistles and the decomposition results of the 3D-SRMD in STFT plane: (**top left**) the real signal; (**top right**) sum of the estimated modes; (**bottom**) the crossover frequency components separation achieved by 3D-SRMD.

To comprehensively evaluate the methods' performance, we also evaluated these methods under different noise levels. The mean output signal-to-noise ratio (SNR) is introduced to measure the accuracy of mode reconstruction as $\frac{1}{K}\sum_{k=1}^{K} 20\log_{10}\left(\frac{\|m_k(t)\|_2}{\|\widehat{m}_k(t)-m_k(t)\|_2}\right)$. Note that the exper-

iments are repeated 100 times at each noise level to obtain average results. As depicted in Fig. 3 (**right**), 3D-SRMD exhibits superior performance at each noise level.

B. Real-World Signal

To demonstrate the effectiveness of 3D-SRMD, a real-world signal from the whistles of the melon-headed whales [30] is employed in this section. The sampling frequency is 48 kHz, while the time duration is 0.04 s. The signal contains crossover frequency components and is contaminated by background noise (see in Fig. 6 (**top left**)). As exhibited in Fig. 6, 3D-SRMD successfully separate the modes with crossover IFs and significantly reduces the background noise, which indicates the potential of our method in practical applications.

V. Conclusion

This paper has proposed an advanced mode decomposition method called 3D-SRMD. By lifting the random feature space to the 3D TFC space, our method is capable of disentangling modes with crossover IFs. Furthermore, a concentrated distribution of random features is also developed to enhance separation accuracy and eliminate the need for clustering algorithms. Finally, 3D-SRMD demonstrates promising performance in both simulated and real-world signals. In the future, we will try to apply the 3D-SRMD in various areas, e.g., radar and biomedical systems. We will also aim to explore model compression techniques to optimize the computational efficiency of 3D-SRMD, enabling its adaptation to large-scale, real-time applications.

References

[1] S. K. Hadjidimitriou and L. J. Hadjileontiadis, "Toward an EEG-based recognition of music liking using time-frequency analysis," *IEEE Transactions on Biomedical Engineering*, vol. 59, no. 12, pp. 3498–3510, 2012.

[2] T. Chen, Q. Zheng, L. Xie, and H. Su, "Sinusoidal-assisted synchrosqueezing transform: Algorithms and biomedical applications," *Biomedical Signal Processing and Control*, vol. 85, p. 105043, 2023.

[3] Z. Feng, M. Liang, and F. Chu, "Recent advances in time–frequency analysis methods for machinery fault diagnosis: A review with application examples," *Mechanical Systems and Signal Processing*, vol. 38, no. 1, pp. 165–205, 2013.

[4] S. Wang, X. Chen, I. W. Selesnick, Y. Guo, C. Tong, and X. Zhang, "Matching synchrosqueezing transform: A useful tool for characterizing signals with fast varying instantaneous frequency and application to machine fault diagnosis," *Mechanical Systems and Signal Processing*, vol. 100, pp. 242–288, 2018.

[5] F. Auger, P. Flandrin, Y.-T. Lin, S. McLaughlin, S. Meignen, T. Oberlin, and H.-T. Wu, "Time-frequency reassignment and synchrosqueezing: An overview," *IEEE Signal Processing Magazine*, vol. 30, no. 6, pp. 32–41, 2013.

[6] N. E. Huang, Z. Shen, S. R. Long, M. C. Wu, H. H. Shih, Q. Zheng, N.-C. Yen, C. C. Tung, and H. H. Liu, "The empirical mode decomposition and the Hilbert spectrum for nonlinear and non-stationary time series analysis," *Proceedings of the Royal Society of London. Series A: mathematical, physical and engineering sciences*, vol. 454, no. 1971, pp. 903–995, 1998.

[7] Z. Wu and N. E. Huang, "Ensemble empirical mode decomposition: a noise-assisted data analysis method," *Advances in adaptive data analysis*, vol. 1, no. 01, pp. 1–41, 2009.

[8] J.-R. Yeh, J.-S. Shieh, and N. E. Huang, "Complementary ensemble empirical mode decomposition: A novel noise enhanced data analysis method," *Advances in adaptive data analysis*, vol. 2, no. 02, pp. 135–156, 2010.

[9] K. Dragomiretskiy and D. Zosso, "Variational mode decomposition," *IEEE transactions on signal processing*, vol. 62, no. 3, pp. 531–544, 2013.

[10] M. Nazari and S. M. Sakhaei, "Successive variational mode decomposition," *Signal Processing*, vol. 174, p. 107610, 2020.

[11] ——, "Variational mode extraction: A new efficient method to derive respiratory signals from ecg," *IEEE journal of biomedical and health informatics*, vol. 22, no. 4, pp. 1059–1067, 2017.

[12] S. Chen, X. Dong, Z. Peng, W. Zhang, and G. Meng, "Nonlinear chirp mode decomposition: A variational method," *IEEE Transactions on Signal Processing*, vol. 65, no. 22, pp. 6024–6037, 2017.

[13] S. Chen, Z. Peng, Y. Yang, X. Dong, and W. Zhang, "Intrinsic chirp component decomposition by using Fourier series representation," *Signal Processing*, vol. 137, pp. 319–327, 2017.

[14] N. Richardson, H. Schaeffer, and G. Tran, "SRMD: Sparse random mode decomposition," *Communications on Applied Mathematics and Computation*, pp. 1–28, 2023.

[15] A. Hashemi, H. Schaeffer, R. Shi, U. Topcu, G. Tran, and R. Ward, "Generalization bounds for sparse random feature expansions," *Applied and Computational Harmonic Analysis*, vol. 62, pp. 310–330, 2023.

[16] E. Saha, H. Schaeffer, and G. Tran, "Harfe: hard-ridge random feature expansion," *Sampling Theory, Signal Processing, and Data Analysis*, vol. 21, no. 2, p. 27, 2023.

[17] S. Mann and S. Haykin, "The chirplet transform: Physical considerations," *IEEE Transactions on Signal Processing*, vol. 43, no. 11, pp. 2745–2761, 1995.

[18] L. Li, N. Han, Q. Jiang, and C. K. Chui, "A chirplet transform-based mode retrieval method for multicomponent signals with crossover instantaneous frequencies," *Digital Signal Processing*, vol. 120, p. 103262, 2022.

[19] C. K. Chui, Q. Jiang, L. Li, and J. Lu, "Analysis of a direct separation method based on adaptive chirplet transform for signals with crossover instantaneous frequencies," *Applied and Computational Harmonic Analysis*, vol. 62, pp. 24–40, 2023.

[20] A. Rahimi and B. Recht, "Weighted sums of random kitchen sinks: Replacing minimization with randomization in learning," *Advances in neural information processing systems*, vol. 21, 2008.

[21] S. S. Chen, D. L. Donoho, and M. A. Saunders, "Atomic decomposition by basis pursuit," *SIAM review*, vol. 43, no. 1, pp. 129–159, 2001.

[22] M. A. Figueiredo, R. D. Nowak, and S. J. Wright, "Gradient projection for sparse reconstruction: Application to compressed sensing and other inverse problems," *IEEE Journal of selected topics in signal processing*, vol. 1, no. 4, pp. 586–597, 2007.

[23] E. Van Den Berg and M. P. Friedlander, "Probing the pareto frontier for basis pursuit solutions," *Siam journal on scientific computing*, vol. 31, no. 2, pp. 890–912, 2009.

[24] E. Van den Berg and M. P. Friedlander, "Sparse optimization with least-squares constraints," *SIAM Journal on Optimization*, vol. 21, no. 4, pp. 1201–1229, 2011.

[25] M. Ester, H.-P. Kriegel, J. Sander, X. Xu *et al.*, "A density-based algorithm for discovering clusters in large spatial databases with noise," in *kdd*, vol. 96, no. 34, 1996, pp. 226–231.

[26] I. Daubechies, J. Lu, and H.-T. Wu, "Synchrosqueezed wavelet transforms: An empirical mode decomposition-like tool," *Applied and computational harmonic analysis*, vol. 30, no. 2, pp. 243–261, 2011.

[27] T. Chen, L. Xie, M. Cui, and H. Su, "Multiple enhanced synchrosqueezing in the time–frequency–chirprate space," *Signal Processing*, vol. 222, p. 109541, 2024.

[28] F. Millioz and N. Martin, "Circularity of the stft and spectral kurtosis for time-frequency segmentation in gaussian environment," *IEEE Transactions on Signal Processing*, vol. 59, no. 2, pp. 515–524, 2010.

[29] S. Chen, X. Dong, G. Xing, Z. Peng, W. Zhang, and G. Meng, "Separation of overlapped non-stationary signals by ridge path regrouping and intrinsic chirp component decomposition," *IEEE Sensors Journal*, vol. 17, no. 18, pp. 5994–6005, 2017.

[30] "Discovery of Sound in the Sea," http://www.dosits.org/.